



Terahertz Time-Domain Spectroscopic (THz-TDS) Insights into Protein Deformation

A. Abouelsayed^{1,2} · Gamal S. El-Bahy¹ · Abdelrazek B. Abdelrazzak¹ 

Received: 20 October 2023 / Accepted: 30 January 2024 / Published online: 12 February 2024
© The Author(s) 2024

Abstract

In this study, we utilized terahertz time-domain spectroscopy (THz-TDS) to study the radiation-induced protein deformation. The absorption coefficient spectra obtained from THz-TDS measurements in the frequency range (0.06–2 THz) was fitted using the Lorentzian model. The absorption coefficient fitting data was used to identify the α -helix and β -structure relative contributions in the protein secondary structure of the kidney tissue of rats irradiated with 10-cGy and 2-Gy X-ray separately or in combination. Our data show that 2-Gy X-irradiation leads to an increase in the β -structure contribution associated with a decrease in the α -helix contribution as indicated by the fitting parameters extracted from fitting the absorption coefficient $\alpha(\omega)$ spectra with the Lorentzian function. The results point out that there is a strong correlation between the strength of the hydrogen bonds located between or inside the polypeptide chains of the extended β -sheet and α -helix, respectively, and the absolute value of the absorption coefficient $\alpha(\omega)$, the refractive index, and the dielectric constant. The lowest refractive index and dielectric constant are recorded in the 2-Gy-irradiated group followed by the 10-cGy–2 Gy-irradiated group while the least effect was recorded in the 10-cGy-irradiated group. These data provide evidence of the adaptive effect of the 10-cGy X-irradiation delivered 24 h prior to the 2-Gy x-irradiation.

Keywords Terahertz time-domain spectroscopy (THz-TDS) · Protein conformation · Ionizing radiation · Radioadaptive response · Lorentz function

1 Introduction

Ionizing radiation is acknowledged for its detrimental effects, especially at high doses [1]. Although the biological effects of low-dose radiation are yet controversial [2–5], it is widely acceptable that low-dose radiation effects are not negligible. The linear no-threshold (LNT) model representing the radiation risk as a function of radiation dose suggests that every radiation dose, however low, carries risk and the risk for every unit dose is constant. Nevertheless, the data showing that low-dose radiation effects are higher than the effects estimated by the LNT model indicate that the LNT model underestimates the low-dose radiation effects

[6–11]. According to recent reports, globally nearly a million patients receive doses in order of 10 cGy as a result of repeated use of radio-imaging [12]. However low, doses of low-LET radiation as low as 10 cGy remain of concern to the radiation protection society [13–15].

Ionizing radiation can affect cell viability and functionality by damaging the cellular macromolecules such as proteins and lipids [11, 16, 17]. We focus here on protein damage by radiation. Proteins are complex molecules responsible for various cellular activities. The protein conformation is a factor that determines the functionality of the protein [18]. Therefore, changes in protein conformation can render the protein nonfunctional. Several characterization methods have been employed to study the protein secondary structure such as FTIR spectroscopy, fluorescence spectroscopy, circular dichroism (CD) spectroscopy [19, 20], nuclear magnetic resonance (NMR) [21], and X-ray diffraction (XRD) [22].

In this study, we utilized the terahertz time-domain spectroscopy (THz-TDS) to inspect the effect of both low- and high-dose radiation on the protein conformation.

✉ Abdelrazek B. Abdelrazzak
a.b.abdelrazzak@gmail.com

¹ Spectroscopy Department, Physics Research Institute, National Research Centre, Cairo 12622, Egypt

² Molecular and Fluorescence Lab, Central Laboratories Network, National Research Centre, Cairo 12622, Egypt

THz-TDS is a modern non-invasive technique, which uses low energy photons in the frequency range between the microwave and the infrared regions [23]. Biological tissues have large absorption in the THz region [24]. The vibrations/rotations of biological molecules involving the intra/inter molecular hydrogen bonds are associated with energies in the THz range [25, 26]. Therefore, THz-TDS can be efficient in studying the biological molecules without inducing damage in them, which was proven by its use in detection and quantification of proteins [27, 28]. Moreover, THz radiation is sensitive to the structure and conformation of proteins [29].

THz-TDS is extensively used for exploration and identification of molecular species via their characteristic vibrational and rotational modes: from diatomic molecules (e.g., CH, CN, CO, FeO, AlCl) up to 13-atomic molecules (e.g., HC₁₀CN) and fullerenes C₆₀ and C₇₀. A huge number of vibrational modes of DNA lie in the frequency range lower than 1 THz [30]. THz-TDS probes allow transitions between various rotational modes in which a dipole moment must exist. Within this study, the optical constants such as the complex refractive index, the absorption coefficient, and the dielectric constant have been extracted from THz measurements. The absorption coefficient is unambiguously determining the attenuation of the THz wave within the sample by absorption, and the refractive index can unambiguously determine the propagation velocity of the wave inside the materials, while the dielectric constant describes the polarizability of the material. In this work, the variation in the optical constants extracted from THz measurements were used to explore the effect ionizing radiation on protein conformation and directly compare the effects of low- and high-dose X-rays.

2 Materials and Methods

2.1 Animal Model

Twenty Sprague-Dawley male rats divided into four groups were used in the study. The different groups are as follows: (1) control (non-irradiated), in which the rats were mock irradiated; (2) 2-Gy-irradiated, in which the rats were 2-Gy X-ray whole-body irradiated; (3) 10-cGy-irradiated, in which the rats were 10-cGy X-ray whole-body irradiated; (4) 10-cGy–2-Gy-irradiated, in which the rats were 10-cGy X-irradiated 24 h prior to a subsequent dose of 2 Gy. Twenty four hours post irradiation, the animals were euthanized and kidney samples collected for investigations.

2.2 Irradiation

Irradiation was performed using a 6-MV linear accelerator (Precise Linear Accelerator; Elekta, Sweden), at a dose rate of 4 Gy/min.

2.3 THz-TDS Investigations

THz measurements were performed using optical laser systems to cover the THz frequency range from 0.06 to 2 THz (TPS Spectra 3000 system; TeraView Ltd., UK). Freeze-dried tissue samples were compressed into thin discs for the THz-TDS measurements. The spectral resolution was 1.2 cm⁻¹, and the number of scans, which have been used throughout all measurements, was 1800 scan/s. In principle, it is possible to use scan rates higher than 1800 scan/s by using a mechanical delay stage in the TPS spectra 3000 system. However, the signal-to-noise ratio is significantly good to fit the absorption coefficient $\alpha(\omega)$ well within the measuring frequency range from 0.06 to 2 THz. Measurements were performed for thin discs of the tissue samples (0.2, 1.2, 0.4, and 0.8 mm for the control and the 2-Gy, 10-cGy, and 10-cGy–2-Gy-irradiated groups, respectively) at room temperature.

The tissue samples were treated as optically thick, and non-birefringent. For normal incidence and by considering that the reflections occur only at the front and at the back interface, see Fig. 1.

The absorption coefficient $\alpha(\omega)$ extracted from THz measurements in the frequency range (0.06–2 THz) was fitted using Lorentz functions according to Eqs. 1 and 2 as described before [31–33]:

$$\epsilon_1 = n^2 - k^2 = \epsilon_\infty + \sum_i \frac{s_i^2(\omega_i^2 - \omega^2)}{(\omega_i^2 - \omega^2)^2 + \Gamma_i^2\omega^2} \quad (1)$$

$$\epsilon_2 = 2nk = \sum_i \frac{s_i^2\Gamma_i\omega}{(\omega_i^2 - \omega^2)^2 + \Gamma_i^2\omega^2} \quad (2)$$

where ω_i is the central frequency, Γ_i is the FWHM, and s_i is the oscillator strength.

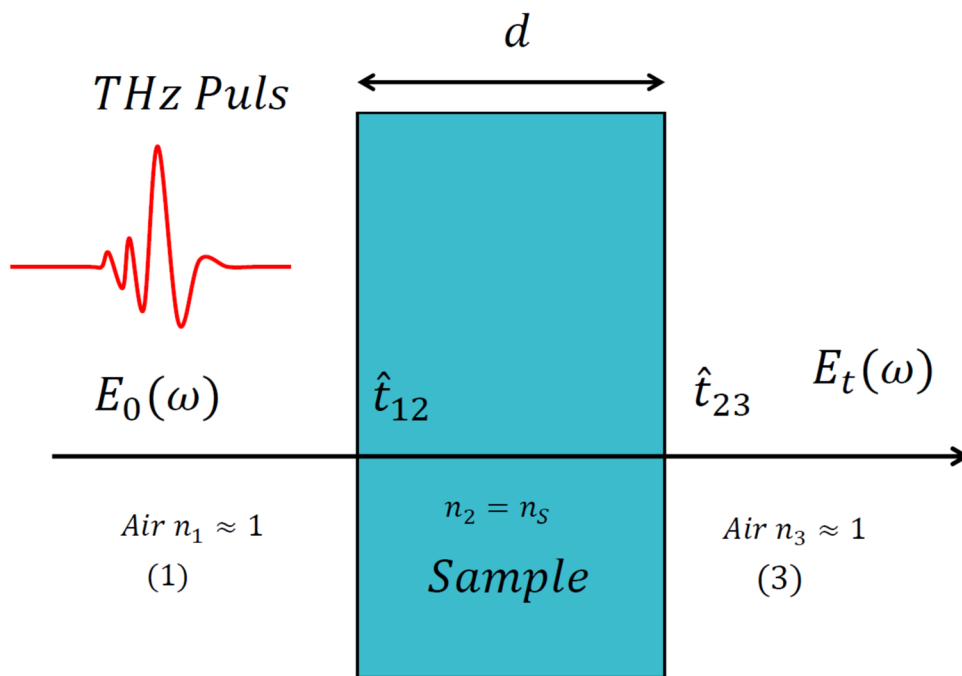
2.4 Ethical Approval

The work was reviewed and approved by the MREC, National Research Centre, Egypt.

3 Results and Discussion

In previous studies [34–37], Fourier transform infrared (FTIR) and dielectric spectroscopy were employed to investigate various radiobiological phenomena using the molecular modification of the biological macromolecules as endpoints. In addition to FTIR and dielectric spectroscopy, THz-TDS was reported to be a sensitive modality for

Fig. 1 Transmission at the air-sample interface



investigating biological molecules [23–25] and the conformational alterations of proteins [38]. In this study, we investigate the deformation in the protein conformation in kidney samples following 10-cGy or/and 2-Gy irradiation using THz-TDS. We investigated and compared the effects of low-dose (10 cGy) and high-dose (2 Gy) radiation on the protein conformation. Moreover, we studied how low-dose irradiation (10 cGy) may influence the effect of a subsequent higher dose irradiation (2 Gy).

Figure 2 a depicts the waveform signals recorded over a 18-ps time window with a spectral resolution of 35 GHz (1.2 cm^{-1}). The temporal waveform was measured through dry nitrogen atmosphere as a reference signal, then the

tissue samples were measured. The corresponding power spectra for dry nitrogen atmosphere and for the samples $|E_{\text{ref}}(\omega)|^2$, $|E_{\text{sam}}(\omega)|^2$ were obtained by applying Fourier transformation to the temporal waveform signal $E_{\text{ref}}(t)$ and $E_{\text{sam}}(t)$ (Fig. 2b). The transmittance phase (the phase difference between the transmitted and the incident waves) is shown in Fig. 2c. Figure 2c shows that the samples irradiated with 10 cGy–2 Gy and 2 Gy show a higher spectral phase as compared to the other two samples (the control and the 10-cGy samples). This is because of the variation of the samples’ thickness. The thickness of the samples irradiated with 10 cGy–2 Gy and 2 Gy is higher than the thickness of the other two samples (the control and the

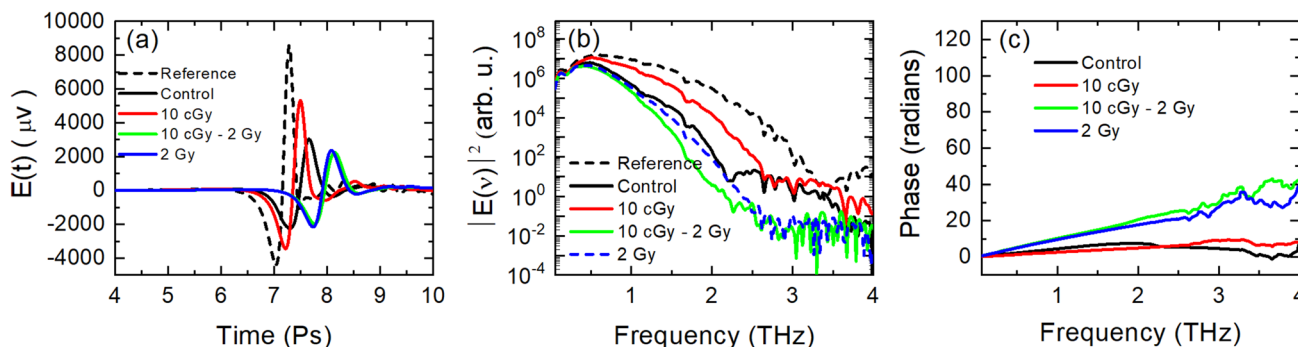


Fig. 2 Response of the tissue samples at THz frequencies. **a** Measured THz electric-field waveforms attenuated through nitrogen and the kidney of the control and the 2-Gy, 10-cGy–2-Gy, and 10-cGy-irradiated groups. **b** The sample spectra: Fourier transforms of the correspond-

ing time-domain signals. **c** The transmittance phase (radians) for the control and the 2-Gy, 10-cGy–2-Gy, and 10-cGy-irradiated groups obtained from the electric field measured by using the THz-TDS laser system in the frequency range 0.06–4 THz

10-cGy samples). The thickness of the samples irradiated with 10 cGy–2 Gy and 2 Gy are 0.8 mm and 1.2 mm, respectively, while the thickness of the control and the irradiated samples with 10 cGy are 0.2 and 0.4 mm, respectively. The data show a remarkable difference between the groups that received 2-Gy and 10-cGy–2-Gy X-rays as compared with the control and 10-cGy-irradiated groups. Based on the available literature [39, 40], the optical constants like the complex refractive index $\tilde{n} = n_s + ik_s$ and the absorption coefficient $\alpha(\omega)$ were extracted from THz transmission data. Both the refractive index $n(\omega)$ and absorption coefficient $\alpha(\omega)$ are obtained from the complex THz transmission data through

$$n(\omega) = 1 + \frac{\varphi(\omega)c}{\omega d} \quad (3)$$

$$\alpha(\omega) = -\frac{2}{d} \ln \left(\frac{(n(\omega) + 1)^2}{4n(\omega)} \times |\tilde{t}(\omega)| \right) \quad (4)$$

Figure 3 shows the absorption coefficient $\alpha(\omega)$ spectra in the THz frequency range 0.06–2 THz of the control and irradiated groups. The control group shows a broad absorption band centered at about 1.14. Above 0.5 THz, the difference between the control and irradiated groups became obvious. A remarkable difference is seen between the 2-Gy, 10-cGy, and 10-cGy–2-Gy-irradiated groups at 2 THz. These data provide indication of the differential effect of low- and high-dose irradiation on the absorption coefficient, which can refer to changes in the molecular structure in the examined samples.

Further, the absorption coefficient $\alpha(\omega)$ spectra of the different groups were fitted via the Lorentz function

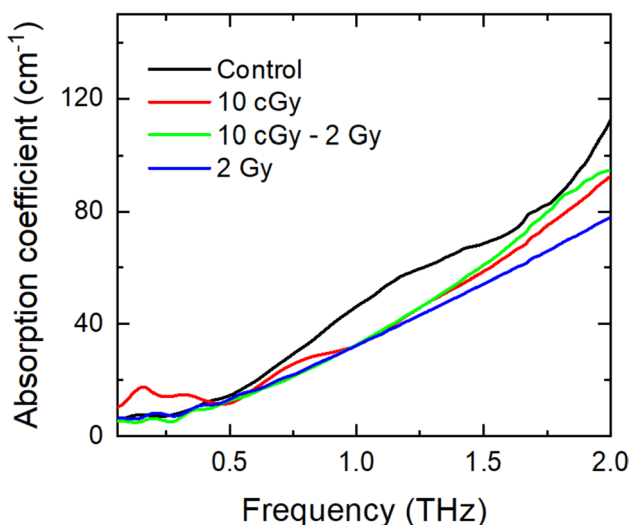


Fig. 3 The absorption coefficient $\alpha(\omega)$ spectra of the kidney of the control and the 2-Gy-, 10-cGy–2-Gy, and 10-cGy-irradiated groups in the THz frequency range 0.06–2 THz

according to the following equation $\alpha(\omega) = \frac{2k(\omega)\omega}{C}$, where the extinction coefficient $k(\omega)$ are related to the imaginary part of the dielectric constant $\epsilon_2(\omega)$ through Eq. 2. The various fitting parameters extracted from fitting of $\alpha(\omega)$ spectra of the different groups are listed in Table 1. For all groups, the $\alpha(\omega)$ spectra were fitted using four Lorentz contributions. These four bands correspond to the different hydrogen bonds between C=O and N–H groups located in the extended β -sheet, α -helix, and antiparallel β -sheet motifs of the protein secondary structure. Meanwhile, random coil and turns/loops motifs are not characterized by having hydrogen bonds [41].

In principle, the strength (the length and direction) of any hydrogen bond depends on the value of the dihedral angles and hence to the chain geometry [42]. Therefore, the hydrogen bonds (in the THz frequency range) appear at different locations in the $\alpha(\omega)$ spectra of different protein secondary structure motifs (extended β -sheet, α -helix, and antiparallel β -sheet). The hydrogen bonds in case of antiparallel β -sheet are so weak [43, 44]. Thus, we attributed the absorption bands between 0.12 and 0.13 THz to the hydrogen bonds of the antiparallel β -sheet motif. The hydrogen bonds, which are inside the polypeptide chains, are related to the α -helix motif. The strength of α -helix hydrogen bonds are modest [45] and therefore located at a higher frequency of about 0.7 THz in the $\alpha(\omega)$ spectra. The strongest hydrogen bonds are in the extended β -sheet [46, 47]. Therefore, we attributed the hydrogen bonds located above 1.4–2 THz to the the extended β -sheet.

According to a previous study by Zhu et al. [48], the protein secondary structure dominated by the α -helix is characterized by two peaks that appear centered at 0.75 and 1.2 THz, while the protein secondary structure dominated by β -sheet has one broad absorption band at 1.35 THz. From Fig. 4a, the control group was fitted with four Lorentz contributions. The Lorentz peaks are listed in Table 1. The absorption peak located at 0.75 is attributed to the α -helix, while the peak at about 1.35–2 THz is attributed to the the extended β -sheets [48]. The α -helix peaks, which appear in the THz frequency range (between 0.7 and 0.75 THz), are due to the alignment of hydrogen bonds inside the α -helix structure in the direction of the THz electric field. In case of β -structures, the hydrogen bonds are located between the polypeptide chains of the β -sheets. Thus, the THz peak corresponds to the alignment of the hydrogen bonds between the polypeptide chains in the direction of the THz electric field.

Fitting the data of the 10-cGy, 10-cGy–2-Gy, and 2-Gy-irradiated groups resulted in two contributions at about 0.12–0.14 THz, 0.7–0.75 THz, and 1.3–2 THz as shown in Fig. 4b–d. The peak at about 0.7–0.75 THz corresponds to α -helix, while the peak at about 1.3–2 THz corresponds to the extended β -sheet. The lower spectral

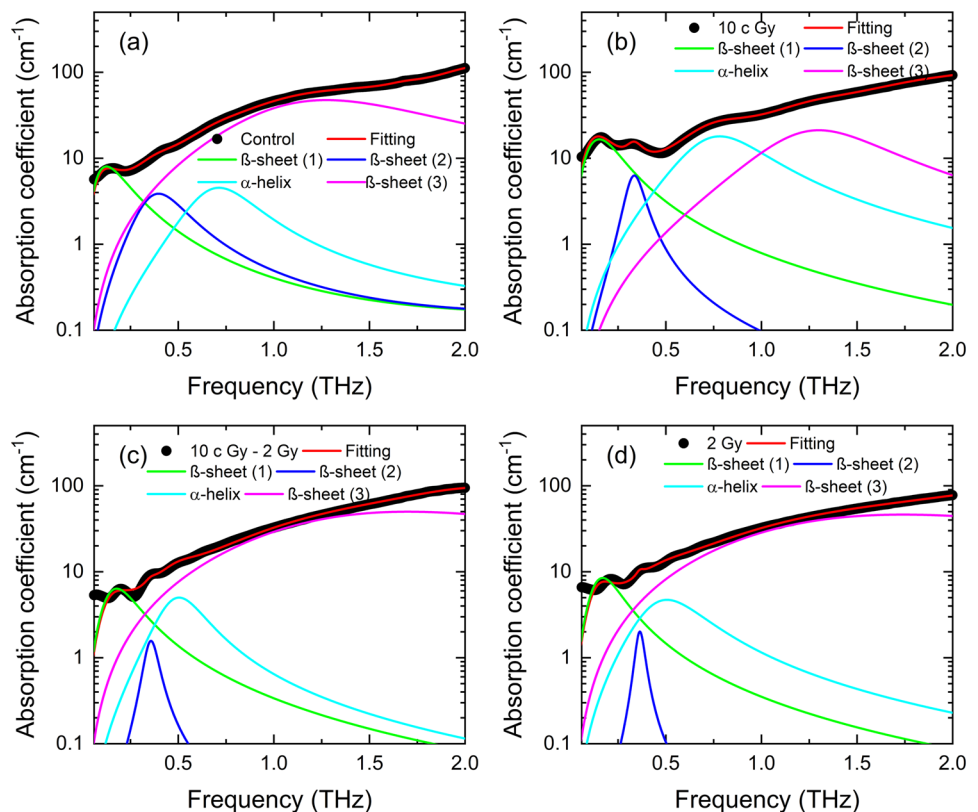
Table 1 The fitting parameters extracted from fitting of the $\alpha(\omega)$ spectra in the THz frequency range of each motif of the protein secondary structure for the control and the 10-cGy-, 2-Gy-, and 10-cGy-2 Gy-irradiated groups

Samples	ω (THz) of hydrogen bond	$\alpha(\omega)$ (cm ⁻¹)	FWHM (THz)	Area	Structure
Control	0.12	8.19	0.21	2.77	Antiparallel β -sheet
	0.39	13.9	0.3	1.92	
	0.71	27.7	0.41	2.87	α -Helix
10 cGy	1.3–2	60.5	1.26	67.67	Extended β -sheet
	0.12	18.8	0.21	5.60	Antiparallel β -sheet
	0.33	15.4	0.11	1.07	
	0.76	27	0.51	13.01	α -Helix
1.3–2	47	0.75	20.66	Extended β -sheet	
10 cGy-2 Gy	0.16	6.7	0.22	2.19	Antiparallel β -sheet
	0.35	10	0.1	0.20	
	0.5	13.7	0.28	2.11	α -Helix
	1.5–2	78.2	2.1	91.18	Extended β -sheet
2 Gy	0.15	9	0.19	2.60	Antiparallel β -sheet
	0.36	10.7	0.1	0.17	
	0.5	15.8	0.42	2.84	α -Helix
	1.6–2	65.7	2.5	88.5892	Extended β -sheet

weight of the alpha-helix band at 0.7–0.75 THz indicates a decrease in the α -helical component of the protein secondary structure. On the other hand, as seen in Fig. 4b–d, the extended β -sheet band originally located at 1.35 THz in the control group was shifted towards a higher frequency of 1.5–2 THz in all irradiated groups with the spectral

weight (area) increasing in the 10-cGy-2-Gy- and 2-Gy-irradiated groups as compared with the control group (see Table 1). These data suggest an increase in the contribution of the β -structure motif at the expense of the α -helical component. These data are concomitant with our previous findings showing a decrease in the α -helix motif and an

Fig. 4 The absorption coefficient $\alpha(\omega)$ spectra together with fitting curve and the fitting contributions using the Lorentz function of kidneys samples of **a** control and the **b** 10-cGy-irradiated, **c** 10-cGy- then 2-Gy-irradiated, and **d** 2-Gy-irradiated groups **a** in the THz frequency range 0.06–2 THz



increase in the β -sheet structures in tissues as a result of exposure to ionizing radiation [37, 49] or lipid peroxidation products [50, 51].

It is obvious from the absolute values of the absorption coefficient $\alpha(\omega)$ listed in Table 1, which is defined as the fraction of THz power radiation absorbed per unit length of the samples, that there is no clear trend for increasing or decreasing the absolute values of $\alpha(\omega)$ due to X-ray irradiation. This is because the hydrogen bonds corresponding to the extended β -sheet, α -helix, and antiparallel β -sheet of the control and the 10-cGy, 10-cGy–2-Gy, and 2-Gy-irradiated groups are mainly located at different THz frequencies in the $\alpha(\omega)$ spectra. It is clear from Fig. 3 that there is an overall increase in the absolute values of $\alpha(\omega)$ spectra with frequency for all groups. These increases are related to all-electron configuration associated with different amide groups which are located in the protein structures.

Despite the increase in $\alpha(\omega)$ spectra with frequency for all groups, the overall absorption coefficients decreased following X-irradiation (Fig. 3). This can be explained as follows: some of partially localized electrons associated with α -helix are transformed to more localized electrons distributed with the extended β -sheet. According a previous study [45], there is a strong correlation between the strength of the hydrogen bond and the electron density distributed over some protein functional groups such as C=O. For the extended β -sheet, the hydrogen bond is extremely strong; thus, a lower electron density is associated with the C=O group. The electrons can flow to or from the C=O group depending on the formation of these very strong hydrogen bonds. In the irradiated groups, a large portion of α -helix (associated with relatively weak hydrogen bonds) are transformed to extended β -sheet (containing strong hydrogen bonds); the electron density is decreased over some protein functional groups and might become more localized. Hence, the overall absolute values of the absorption coefficient $\alpha(\omega)$ decreased in the irradiated groups.

Further information has been obtained by linear fitting of the $\alpha(\omega)$ spectra of the control and the 10-cGy-, 10-cGy–2-Gy-, and 2-Gy-irradiated groups in the frequency range 0.2–2.0 THz. The fitted lines are drawn in dotted lines, and the slopes of these lines are represented by a set of linear equations (Fig. 5). The control, which contains the highest portion of α -helix, shows the largest slope about 0.56 ± 0.04 ($\times 10^2 \text{ cm}^{-1} \text{ THz}^{-1}$), while the 2-Gy-irradiated group, which contains mainly a large portion of β -sheets, shows a small slope value of about 0.41 ± 0.02 ($\times 10^2 \text{ cm}^{-1} \text{ THz}^{-1}$). The 10-cGy and 10-cGy–2-Gy groups show a modest slope between the control and 2-Gy groups, where the slopes are 0.5 ± 0.03 ($\times 10^2 \text{ cm}^{-1} \text{ THz}^{-1}$) and 0.53 ± 0.01 ($\times 10^2 \text{ cm}^{-1} \text{ THz}^{-1}$) for the two samples, respectively. The recovery of the value of the slope in the 10-cGy–2-Gy group as compared with the 2-Gy-irradiated group suggests an adaptive

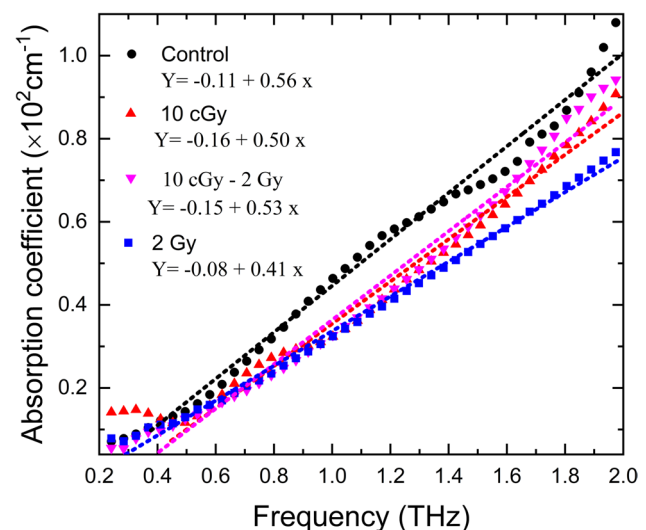


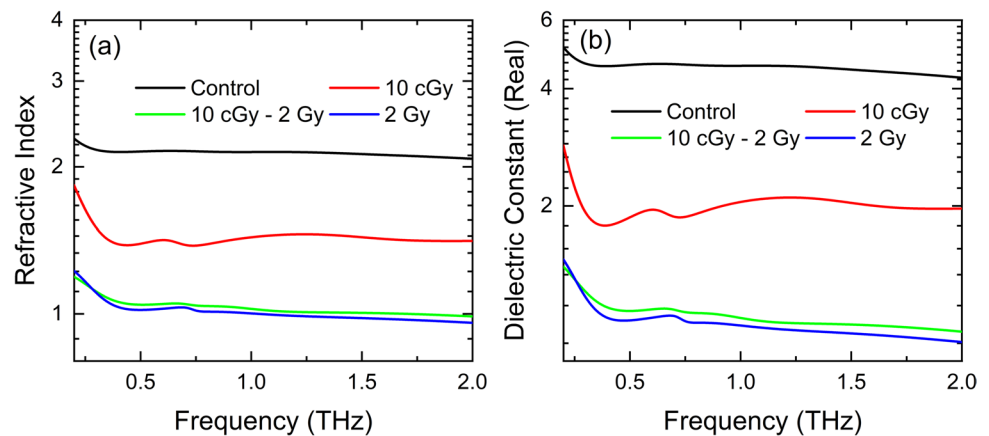
Fig. 5 The linear fitting of the absorption coefficient (m^{-1}) of the control and the 2-Gy-, 10-cGy–2-Gy-, and 10-cGy-irradiated groups in the frequency range 0.2–2 THz. The fitted lines are represented by a set of linear equations

response of the 10-cGy irradiation given prior to a 2-Gy dose. Our results are in consistency with the results obtained by Dorney and Wu et al. [39, 52], in which the highest slope of $\alpha(\omega)$ was reported for the reconstituted silk fibroin, which contains a large portion of α -helix configurations, while the smallest slope is recorded for degummed silk which contains a large portion of β -sheets.

To further confirm our findings, the changes in the real part of the refractive index and the real part of the dielectric constant were investigated in the THz frequency range (0.2–2 THz) (Fig. 6a, b). Figure 6 shows that both the refractive index and dielectric constant decrease monotonically throughout the whole frequency range (0.2–2 THz) in all of the irradiated groups as compared with the control group. The refractive index can unambiguously determine the propagation velocity of the wave inside the materials, while the dielectric constant describes the polarizability of the material. Therefore, both of the refractive index and the dielectric constant can provide information on the conformation of the protein. The lowest refractive index and dielectric constant are recorded in the 2-Gy-irradiated group followed by the 10-cGy–2-Gy-irradiated group while the least effect was recorded in the 10-cGy-irradiated group.

Physically, the absolute value of the dielectric constant reflects the response of medium to the applied electric field. Therefore, the decrease in the dielectric constant means the lower response of the medium to the applied electric field. In our case here, the dipole moment and hence dielectric constant are highly correlated to the strength of the hydrogen bonds between the polypeptide chains forming the secondary structure of the protein. The absorption coefficient

Fig. 6 **a** The real part of the refractive index spectra and **b** the real part of the dielectric constant of rat kidneys of the control and the 2-Gy-, 10-cGy-, 2-Gy-, and 10-cGy-irradiated groups in the frequency range 0.06–2 THz



data reveal larger contribution from the β -structure motif in all of the irradiated groups. The decrease in the dielectric constant in the irradiated groups, in which the β -structure contribution is higher, reflects the role of the strength hydrogen bonds, interconnecting the polypeptide chains, on the absolute values of the dielectric constant. As the samples are exposed to X-ray radiation, a large portion of the α -helix (associated with relatively weak hydrogen bonds) are transformed to the extended β -sheet (containing strong hydrogen bonds); the electron densities are decreased over some portion of protein functional groups and might become more localized. Hence, the overall absolute values of the dielectric constant are decreased. Thus, the decrease in the dielectric constant in the irradiated groups, in which the β -structure shows higher contribution than the control group, may provide an indication that their response to the applied electric field is lower than that of the control sample in which the α -helix dominated.

The data in Fig. 6 show that 2-Gy irradiation leads to the highest decrease in the refractive index and the dielectric constant. However, a lower dose (10 cGy) given 24 h prior to the 2-Gy dose leads to a lessening in the effect of a higher dose (2 Gy) as indicated by the increase in the dielectric constant and refractive index values in the whole frequency range. These data may provide an indication of radioadaptation induced by the 10-cGy irradiation given prior to the 2-Gy irradiation. These data are concomitant with previous findings by our group [33] in which FTIR spectroscopy provided evidence of radioadaptation induced by a dose of 100 mGy given 24 h prior to a subsequent 2-Gy dose of X-ray.

4 Conclusions

Ionizing radiation instigated a differential increase in the β -structure motif contribution in the protein secondary structure at the cost of the α -helical component in kidney tissue

samples. Changes in protein conformation following irradiation were evident by THz-TDS. Although 2-Gy irradiation leads to the most significant modification in the protein conformation, 10-cGy irradiation delivered 24 h prior to 2-Gy irradiation leads to a reduction in the effect of 2-Gy irradiation on the protein conformation. This gives an indication of a possible adaptation effect of the 10-cGy irradiation. The 10-cGy irradiation evidently modified the protein conformation.

Author Contribution A.A. performed the fitting analysis and contributed to the manuscript writing. G.E. Contributed to the data analysis and manuscript revision. A.B.A. performed the experimental work and data analysis and wrote and reviewed the main manuscript text.

Funding Open access funding provided by The Science, Technology & Innovation Funding Authority (STDF) in cooperation with The Egyptian Knowledge Bank (EKB). National Research Centre, 13020305, Abdelrazek Abdelrazzak.

Data Availability The datasets used and/or analyzed during the current study available from the corresponding author on reasonable request.

Declarations

Competing Interests The authors declare no competing interests.

Open Access This article is licensed under a Creative Commons Attribution 4.0 International License, which permits use, sharing, adaptation, distribution and reproduction in any medium or format, as long as you give appropriate credit to the original author(s) and the source, provide a link to the Creative Commons licence, and indicate if changes were made. The images or other third party material in this article are included in the article's Creative Commons licence, unless indicated otherwise in a credit line to the material. If material is not included in the article's Creative Commons licence and your intended use is not permitted by statutory regulation or exceeds the permitted use, you will need to obtain permission directly from the copyright holder. To view a copy of this licence, visit <http://creativecommons.org/licenses/by/4.0/>.

References

- E.J. Hall, A.J. Giaccia, *Radiobiology for the radiologist*, 6th edn. (Lippincott Williams & Wilkins, Philadelphia, 2006), p. 597
- W.F. Morgan, W.J. Bair, Issues in low dose radiation biology: the controversy continues. A perspective. *Radiat. Res.* **179**, 501–510 (2013)
- E. Shin, S. Lee, H. Kang, J. Kim, K. Kim, H. Youn, Y.W. Jin, S. Seo, B. Youn, Organ-specific effects of low dose radiation exposure: a comprehensive review. *Front. Genet.* **11**, 566244 (2020)
- F.R. Tang, W.K. Loke, B.C. Khoo, Low-dose or low-dose-rate ionizing radiation-induced bioeffects in animal models. *J. Radiat. Res.* (2017)
- J. Cui, G. Yang, Z. Pan, Y. Zhao, X. Liang, W. Li, L. Cai, Hormetic response to low-dose radiation: focus on the immune system and its clinical implications. *Int. J. Mol. Sci.* **18**, 280 (2017)
- A. Deshpande, E. Goodwin, S. Bailey, B. Marrone, B. Lehnert, thE, Alpha-particle-induced sister chromatid exchange in normal human lung fibroblasts: evidence for an extranuclear target. *Radiat. Res.* **145**, 260–267 (1996)
- M.A. Hill, D.L. Stevens, M. Kadhim, M. Blake-James, A.J. Mill, D.T. Goodhead, Experimental techniques for studying bystander effects in vitro by high and low-LET ionising radiation. *Radiat. Prot. Dosimetry* **122**, 260–265 (2006)
- M.A. Kadhim, R. Lee, S.R. Moore, D.A. Macdonald, K.L. Chapman, G. Patel, K.M. Prise, Genomic instability after targeted irradiation of human lymphocytes: evidence for inter-individual differences under bystander conditions. *Mutat. Res.* **688**, 91–94 (2010)
- I. Koturbash, J. Loree, K. Kutanzi, C. Koganow, I. Pogribny, O. Kovalchuk, In vivo bystander effect: cranial X-irradiation leads to elevated DNA damage, altered cellular proliferation and apoptosis, and increased p53 levels in shielded spleen. *Int. J. Radiat. Oncol. Biol. Phys.* **70**, 554–562 (2008)
- I. Koturbash, M. Merrifield, O. Kovalchuk, Fractionated exposure to low doses of ionizing radiation results in accumulation of DNA damage in mouse spleen tissue and activation of apoptosis in a p53/Atm-independent manner. *Int. J. Radiat. Biol.* **93**, 148–155 (2017)
- A.A. Mohye El-Din, A.B. Abdelrazzak, M.T. Ahmed, M.A. El-Missiry, Radiation induced bystander effects in the spleen of cranially-irradiated rats. *Br. J. Radiol.* **90**, 20170278 (2017)
- W. Rühm, D. Laurier, R. Wakeford, Cancer risk following low doses of ionising radiation—current epidemiological evidence and implications for radiological protection. *Mutat. Res. Genet. Toxicol. Environ. Mutagen.* **873**, 503436 (2022)
- M. Doss, Future of radiation protection regulations. *Health Phys.* **110**, 274–275 (2016)
- R.A. Britten, A. Fesshaye, A. Tidmore, A.A. Blackwell, Similar loss of executive function performance after exposure to low (10 CGy) doses of single (4He) ions and the multi-ion GCRSim beam. *Radiat. Res.* **198**, 375–383 (2022)
- S. Stephenson, A. Liu, A.A. Blackwell, R.A. Britten, Multiple decrements in switch task performance in female rats exposed to space radiation. *Behav. Brain Res.* **449**, 114465 (2023)
- A.B. Abdelrazzak, P. O'Neill, M.A. Hill, Intercellular induction of apoptosis signalling pathways. *Radiat. Prot. Dosimetry* **143**, 289–293 (2011)
- A.B. Abdelrazzak, D.L. Stevens, G. Bauer, P. O'Neill, M.A. Hill, The role of radiation quality in the stimulation of intercellular induction of apoptosis in transformed cells at very low doses. *Radiat. Res.* **176**, 346–355 (2011)
- C.M. Dobson, Protein folding and misfolding. *Nature* **426**, 884–890 (2003)
- X. Zhao, Y. Wang, D. Zhao, Structural analysis of biomacromolecules using circular dichroism spectroscopy. *Advanced Spectroscopic Methods to Study Biomolecular Structure and Dynamics.* p.77–103 (2023)
- A. Buckley, J. Warren, R. Hussain, R. Smith, Synchrotron radiation circular dichroism spectroscopy reveals that gold and silver nanoparticles modify the secondary structure of a lung surfactant protein B analogue. *Nanoscale* **15**, 4591–4603 (2023)
- A.H. Moraes, A.P. Valente, Conformational dynamics and kinetics of protein interactions by nuclear magnetic resonance. *J. Magn. Reson. Open* **14**, 100093 (2023)
- A. Zochedh, A. Shunmuganarayanan, A.B. Sultan, Conformational fidelity and hydrogen bond associability of L-histidine with sulfamate anion studied through XRD, quantum chemical, spectroscopic and molecular docking simulation as a cdk-4 inhibitor against retinoblastoma. *J. Mol. Struct.* **1274**, 134402 (2023)
- R.J. Falconer, A.G. Markelz, Terahertz spectroscopic analysis of peptides and proteins. *J. Infrared Millim. Terahertz Waves.* **33**, 973–988 (2012)
- A. Fitzgerald, E. Berry, N. Zinov'ev, S. Homer-Vanniasinkam, R. Miles, J. Chamberlain, M. Smith, Catalogue of human tissue optical properties at terahertz frequencies. *J. Biol. Phys.* **29**, 123–128 (2003)
- P.U. Jepsen, D.G. Cooke, M. Koch, Terahertz spectroscopy and imaging—modern techniques and applications. *Laser Photonics Rev.* **5**, 124–166 (2011)
- W.E. Baughman, H. Yokus, S. Balci, D.S. Wilbert, P. Kung, S.M. Kim, Observation of hydrofluoric acid burns on osseous tissues by means of terahertz spectroscopic imaging. *IEEE Trans. Terahertz Sci. Technol.* **3**, 387–394 (2013)
- L. Xie, W. Gao, J. Shu, Y. Ying, J. Kono, Extraordinary sensitivity enhancement by metasurfaces in terahertz detection of antibiotics. *Sci. Rep.* **5**, 8671 (2015)
- Y. Peng, C. Shi, M. Xu, T. Kou, X. Wu, B. Song, H. Ma, S. Guo, L. Liu, Y. Zhu, Qualitative and quantitative identification of components in mixture by terahertz spectroscopy. *IEEE Trans. Terahertz Sci. Technol.* **8**, 696–701 (2018)
- C.C. Cooksey, B.J. Greer, E.J. Heilweil, Terahertz spectroscopy of l-proline in reverse aqueous micelles. *Chem. Phys. Lett.* **467**, 424–429 (2009)
- F. Merzel, F. Fontaine-Vive, M. Johnson, G. Kearley, Atomistic model of DNA: phonons and base-pair opening. *Phys. Rev. E* **76**, 031917 (2007)
- A. Abouelsayed, N. Ghazal, W. Eisa, B. Anis, Exploring the conduction mechanism of PEDOT: PSS free-standing thin films doped with SWCNTs: THz and infrared-ultraviolet spectroscopy study. *Carbon* **197**, 10–17 (2022)
- H. Afify, S. Hassan, B. Anis, A. Abouelsayed, Effect of UV light illumination in humid air on the optical and electronic properties of the orthorhombic α -MoO₃ and monoclinic β -MoO₃. *J. Appl. Phys.* **132**, 075102 (2022)
- A. Abouelsayed, G.S. El-Bahy, A.B. Abdelrazzak, FTIR spectroscopic investigations of protein conformation provide clues of radioadaptation in the kidney of low-dose irradiated rats. *J. Mol. Struct.* **1295**, 136643 (2024)
- A.B. Abdelrazzak, G.S. El-Bahy, FT-IR spectroscopic investigation of ionizing radiation-induced damage in the small intestine of whole-body irradiated rats. *Vib. Spectrosc.* **99**, 146–150 (2018)
- A.B. Abdelrazzak, A. Hezma, G.S. El-Bahy, ATR-FTIR spectroscopy probing of structural alterations in the cellular membrane of abscopal liver cells. *Biochim. Biophys. Acta Biomembr.* (1863), 183726 (2021)
- A.B. Abdelrazzak, A.M. Labeeb, G.S. El-Bahy, Changes in the dielectric properties of rat lung tissue following x-irradiation. *Egypt. J. Basic Appl. Sci.* **5**, 298–302 (2018)

37. A. Abouelsayed, A. Hezma, G.S. El-Bahy, A.B. Abdelrazzak, Modification of protein secondary structure as an indicator of radiation-induced abscopal effect: a spectroscopic investigation. *Spectrochim. Acta Part A Mol. Biomol. Spectrosc.* **287**, 122093 (2023)
38. A. Markelz, S. Whitmire, J. Hillebrecht, R. Birge, THz time domain spectroscopy of biomolecular conformational modes. *Phys. Med. Biol.* **47**, 3797 (2002)
39. T.D. Dorney, R.G. Baraniuk, D.M. Mittleman, Material parameter estimation with terahertz time-domain spectroscopy. *JOSA A* **18**, 1562–1571 (2001)
40. L. Duvillaret, F. Garet, J.-L. Coutaz, A reliable method for extraction of material parameters in terahertz time-domain spectroscopy. *IEEE J. Sel. Top. Quantum Electron.* **2**, 739–746 (1996)
41. M. Jackson, H.H. Mantsch, Beware of proteins in DMSO. *Biochim. Biophys. Acta, Prot. Struct. Mol. Enzymol.* **1078**, 231–235 (1991)
42. M. Jackson, H.H. Mantsch, Protein secondary structure from FT-IR spectroscopy: correlation with dihedral angles from three-dimensional Ramachandran plots. *Can. J. Chem.* **69**, 1639–1642 (1991)
43. T. Miyazawa, The characteristic band of secondary amides at 3100 cm⁻¹. *J. Mol. Spectrosc.* **4**, 168–172 (1960)
44. W. Moore, S. Krimm, Transition dipole coupling in amide I modes of β polypeptides. *Proc. Natl. Acad. Sci.* **72**, 4933–4935 (1975)
45. M. Jackson, H.H. Mantsch, The use and misuse of FTIR spectroscopy in the determination of protein structure. *Crit. Rev. Biochem. Mol. Biol.* **30**, 95–120 (1995)
46. D.M. Byler, J.M. Purcell, FTIR examination of thermal denaturation and gel-formation in whey proteins, 7th Intl Conf. on Fourier Transform Spectroscopy SPIE. 415–417 (1989)
47. A. Clark, D. Saunderson, A. Suggett, Infrared and laser-Raman spectroscopic studies of thermally-induced globular protein gels. *Int. J. Pept. Protein Res.* **17**, 353–364 (1981)
48. Z. Zhu, Y. Bian, X. Zhang, R. Zeng, B. Yang, Evaluation of formation and proportion of secondary structure in γ -polyglutamic acid by terahertz time-domain spectroscopy. *Spectrochim. Acta Part A Mol. Biomol. Spectrosc.* **271**, 120940 (2022)
49. P. Demir, S.B. Akkas, M. Severcan, F. Zorlu, F. Severcan, Ionizing radiation induces structural and functional damage on the molecules of rat brain homogenate membranes: a Fourier transform infrared (FT-IR) spectroscopic study. *Appl. Spectrosc.* **69**, 154–164 (2015)
50. K.V. Ramana, S. Srivastava, S.S. Singhal, Lipid peroxidation products in human health and disease. *Oxid. Med. Cell. Longev.* **2013** (2013)
51. M. Corinne, Spickett, Andrew R. Pitt, Modification of proteins by reactive lipid oxidation products and biochemical effects of lipoxidation. *Essays Biochem.* **64**, 19–31 (2019)
52. X. Wu, X. Wu, M. Shao, B. Yang, Structural changes of Bombyx mori fibroin from silk gland to fiber as evidenced by Terahertz spectroscopy and other methods. *Int. J. Biol. Macromol.* **102**, 1202–1210 (2017)

Publisher's Note Springer Nature remains neutral with regard to jurisdictional claims in published maps and institutional affiliations.